Design and Experimental Investigation of a Nondestructive Hydrogen-Detection Device Based on Backscattering Detector Layout via Neutron Incoherent Scattering

Yifan Liu(刘一璠)[1]， Guanyun Yan（闫冠云）[1,‡]，Xiaoqiu Ye（叶小球）[2] ，Zongyue Wang（王宗悦）[1]，Heyong Huo（霍合勇）[1]，Siyu Chen（陈思宇）[1]，Xin Yang（杨鑫）[1]，Feng Yang（杨峰）[1]，Beibei Pang（庞蓓蓓）[1]，Jingyao Xie（解景尧)[1]，Xiangqian Peng（彭湘黔）[2]，Ting Zhang（张婷）[2]， and Guangai Sun（孙光爱）[1,†]

[1]*National Key Laboratory of Neutron Science and Technology, Institute of Nuclear Physics and Chemistry, Chinese Academy of Engineering Physics, Mianyang 621999, Sichuan, China*

[2]*Institute of Materials, China Academy of Engineering Physics, Jiangyou 621907, China*

Hydrogen plays a crucial role in the evolution of material properties; however, its precise, non-destructive quantitative detection in materials remains a challenge in the field of materials science. Utilizing the characteristic of hydrogen having an extremely high neutron incoherent scattering cross-section, a dedicated device for non-destructive hydrogen detection was developed in this study. The device employs a backscattering detector layout to prevent interference from strong forward stray signals of the incident neutron beam, utilizes an ultra-short sample-to-detector distance to significantly enhance testing efficiency, and adopts a long-wavelength neutron testing mode to eliminate the influence of intrinsic material variations. Experimental tests on polypropylene (PP) thin-film standard samples with known hydrogen content demonstrate an excellent linear relationship between the measured neutron count rate and the hydrogen content. The application of this method to hydrogen measurement in zirconium alloys shows that it can sensitively determine the hydrogen content in materials, with a theoretical limit of detection of approximately 3.3 ppm for zirconium alloy samples. This study provides a novel, non-destructive, and sensitive testing approach for hydrogen measurement.

Keywords: Neutron incoherent scattering; Hydrogen quantification; Polypropylene thin films; Low-concentration hydrogen analysis
PACS: 61.05.fg, 07.85.Nc

1. Introduction

Hydrogen has the smallest atomic number and is a fundamental element of

[†]Corresponding author. E-mail: guangaisun_80@163.com
[‡]Corresponding author. E-mail: yanguany@126.com

matter[1], existing in almost all organic, inorganic, and metallic materials. In high-strength metallic materials, trace amounts of hydrogen can cause hydrogen embrittlement fracture under stress levels far below the yield strength[2]; in semiconductor materials, strict quantification of hydrogen enables optimal performance[3]; in the production of specialty glass, determining the hydrogen content allows for precise assessment of hydroxyl content, thereby finely controlling the refractive index profile[4]. However, how to accurately determine the hydrogen content in materials has always been an unavoidable problem in materials science research[5].

Thermogravimetric Analysis (TGA)[6] and Thermal Desorption Spectroscopy (TDS)[7] utilize heating to cause hydrogen to escape from within the material, enabling the analysis of hydrogen content by evaluating the weight difference before and after desorption or the amount of hydrogen in the evolved gas; however, they cannot provide spatial distribution information of hydrogen within the sample[8]. Techniques such as Atom Probe Tomography (APT)[9] and Secondary Ion Mass Spectrometry (SIMS)[10] can achieve nanoscale and microscale spatial resolution of hydrogen in materials, obtaining localized distribution information near defects, interfaces, and precipitates[11]. Nevertheless, the sample preparation or testing processes of these methods disrupt the original state of the sample; given the high mobility of hydrogen[12], this adversely affects the analysis of its true state[13]. Ultrasonic Testing (UT)[14] is primarily used to detect phenomena such as hydrogen-induced cracking, hydrogen embrittlement, and hydride damage in large components; fundamentally, it is an indirect detection method based on monitoring variations in the material's density, making sensitive analysis of hydrogen content difficult to achieve[8]. X-ray Photoelectron Spectroscopy (XPS)[15] can analyze surface chemical shifts and elemental valence state evolution, but its limited penetration depth hinders quantitative analysis of bulk hydrogen content[16]; Nuclear Magnetic Resonance (NMR)[17] spectroscopy offers high sensitivity for hydrogen-containing organic systems, yet its application in metallic systems is severely restricted by the electromagnetic shielding effect caused by free electrons[18].

Neutrons are highly sensitive to hydrogen, possessing deep penetration and non-destructive testing capabilities, which makes them an ideal probe for hydrogen analysis[19]. Different neutron techniques correspond to macro-distribution, quantitative content, microstructure, and dynamics across various scales and dimensions in hydrogen behavior research, exhibiting excellent complementarity[20]. Neutron Reflectometry (NR)[21] can obtain depth-distribution information of hydrogen in thin films and at interfaces by analyzing reflectivity curves, whereas Quasi-Elastic Neutron Scattering (QENS)[22, 23] enables the study of hydrogen diffusion dynamics through energy broadening analysis. Coherent elastic scattering-based techniques—namely Neutron Diffraction (ND)[24] and Small-Angle Neutron Scattering (SANS)[25]—are employed to analyze hydrogen-induced crystal structure changes and nanoscale structural evolution, respectively. Neutron Imaging (NI)[19, 26] visualizes the spatial distribution of hydrogen by measuring the attenuation of neutron intensity as the beam passes through the sample, and it has been widely applied in in

situ studies of hydrogen diffusion and hydride corrosion processes in zirconium alloys. Nevertheless, certain large components or materials that neutrons cannot easily penetrate cannot be evaluated using this method[27].

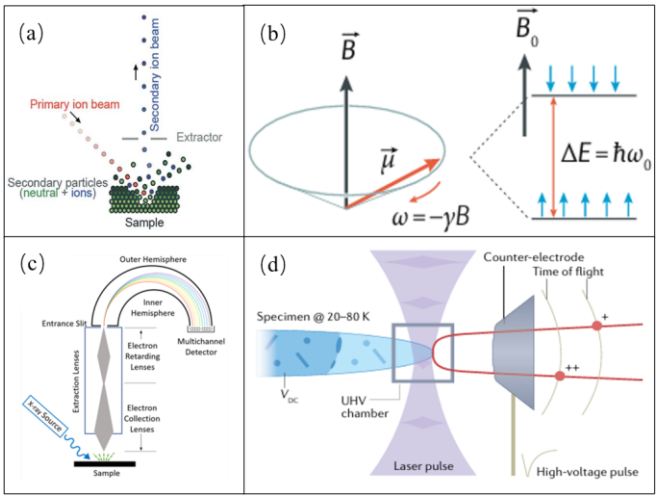


Fig. 1. Schematic illustration of the principles of different hydrogen characterization techniques: (a) SIMS[28], (b)NMR[29], (c) XPS[30], and (d) APT[31].

Incoherent Neutron Scattering[32] techniques utilize the exceptionally high neutron incoherent scattering cross-section of hydrogen to achieve quantitative analysis of hydrogen content. Due to its broader signal collection angle, Incoherent Neutron Scattering is suitable for measuring hydrogen content in large components or materials that neutrons cannot easily penetrate[33]. Currently, international attempts have been made to analyze hydrogen content in materials using neutron diffractometers and wide-angle neutron scattering spectrometers[32]. However, the background neutron scattering obtained is complex, and the ability to discriminate hydrogen-related signals as well as the signal-to-noise ratio remain poor[34]. The primary reason is that conventional neutron scattering instrument designs typically treat the incoherent background signal of hydrogen as a detrimental factor to be eliminated[34], resulting in the low testing efficiency reported in previous studies. To date, no dedicated instrument design specifically optimized for hydrogen content measurement has been reported.

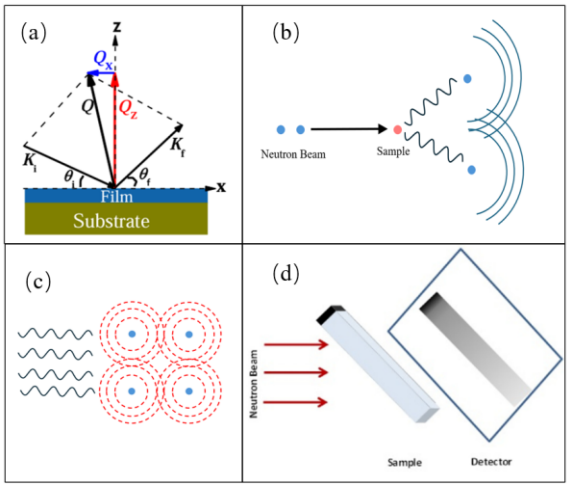


Fig. 2. Schematic illustration of the principles of different neutron characterization

techniques: (a) NR[35], (b)Incoherent Neutron Scattering, (c) ND, and (d) NI[33].

In this study, a neutron scattering apparatus for non-destructive testing of hydrogen was developed, in which the detector layout, scattering angles, and neutron wavelength parameters for incoherent scattering were designed and optimized. The performance of the apparatus was experimentally validated using polypropylene (PP) thin-film standard samples and hydrogen-containing zirconium alloy samples. The experimental results demonstrate that the apparatus can effectively enhance the detection sensitivity and testing efficiency for hydrogen.

2. Technical Principles

Because neutrons carry no electric charge, they possess extremely strong penetrability, allowing them to penetrate deep into the interior of matter and interact strongly with atomic nuclei. The primary types of neutron-nucleus interactions include nuclear absorption, incoherent scattering on individual atomic nuclei, and coherent scattering on the crystal lattice. Its microscopic total cross-section σ_{tot} can be expressed as[36]:

$$\sigma_{\mathrm{tot}} = \sigma_{\mathrm{a}} + \sigma_{\mathrm{s}} = \sigma_{\mathrm{a}} + \sigma_{\mathrm{inc}} + \sigma_{\mathrm{coh}}, \tag{1}$$

Where σ_{a} is the absorption cross-section, σ_{s} is the total scattering cross-section, and σ_{inc} and σ_{coh} represent the incoherent scattering cross-section and coherent scattering cross-section, respectively. Under the approximation of low absorption and low multiple scattering, when an incident neutron beam with a flux f passes through a single atomic nucleus, the total neutron count N received per unit time by a neutron detector with an effective area of S at a distance R from the sample is given by[37]:

$$N = fN_{\mathrm{A}}\left(\frac{m_H}{M_H}\sigma_{\mathrm{s}}^{\mathrm{H}} + \sum_i \frac{m_i}{M_i}\sigma_{\mathrm{s}}^{i}\right)\cdot\frac{S}{4\pi R^2}, \tag{2}$$

where N_{A} is the Avogadro constant; m_H, M_H, and $\sigma_{\mathrm{s}}^{\mathrm{H}}$ represent the mass and molar mass, and total scattering cross-section of the hydrogen element in the sample, respectively; and m_i, M_i, and σ_s^i denote mass and molar mass, and total scattering cross-section of the matrix element i, respectively. To quantitatively characterize the hydrogen content, the mass concentration of the hydrogen element, C_H, is defined as the ratio of the hydrogen mass to the total mass of the matrix:

$$C_{\mathrm{H}} = \frac{m_H}{\sum_i m^i}, \tag{3}$$

Substituting Eq. (3) into Eq. (2) and dividing both sides of the equation by the incident neutron flux f for intensity normalization, we obtain:

$$I = \frac{N}{f} = N_{\mathrm{A}}\cdot\left(\sum_i m_i\right)\frac{\sigma_{\mathrm{s}}^{\mathrm{H}}}{M_H}\frac{S}{4\pi R^2}\cdot C_H + N_{\mathrm{A}}\cdot\left(\sum_i \frac{m_i}{M_i}\sigma_{\mathrm{s}}^{i}\right)\frac{S}{4\pi R^2}, \tag{4}$$

Since the incoherent scattering cross-section of hydrogen is significantly larger than its coherent scattering cross-section as well as the incoherent scattering cross-sections of common substrate materials[37], the second term in Eq. (4), which does not contain hydrogen can be regarded as a constant background under real experimental conditions with a fixed sample matrix and specified parameters. Under

these conditions, the normalized scattering intensity I exhibits a linear correlation with the hydrogen concentration，where A corresponds to the sensitivity coefficient of the system for hydrogen detection, and the intercept B represents the comprehensive background value derived from both ambient background and sample matrix scattering.

$$I = AC_{\mathrm{H}} + B \tag{5}$$

The quantitative model adopted in this study is established on the assumption of weak neutron absorption and multiple scattering effects in the sample. However, for materials with a high macroscopic absorption cross-section or a large sample thickness, the neutron flux that actually participates in scattering and is received by the detector decreases, causing the measurement results to typically deviate from the ideal linear relationship[38]. Therefore, for high-absorption materials, such as materials containing high-absorption elements like B or Li, the neutron attenuation can be mitigated by reducing the sample thickness, or the deviations caused by absorption effects can be corrected based on specific materials and geometric conditions[39]:

$$C_{\mathrm{H}} = C_{\mathrm{Hobs}} \cdot e^{\mu_{\mathrm{abs}} \cdot x(sec\alpha - 1)} \tag{6}$$

Where C_{Hobs} is the apparent mass concentration of hydrogen calculated from the signal intensity obtained by the detector, μ_{abs} is the macroscopic absorption coefficient of the sample, x is the sample thickness, and α is the geometric angle related to the experimental setup. When the multiple scattering effect caused by high-capacity hydrogen storage materials (such as borohydrides or lithium-based hydrides) cannot be neglected, the incoherent scattering intensity may exhibit a non-linear response or even approach saturation. In this case, a correction model considering both neutron attenuation and multiple scattering effects should be adopted, where ρ is the number density of the sample[40]:

$$C_{\mathrm{H}} = C_{\mathrm{Hobs}} \cdot \frac{e^{x\rho\sigma_{\mathrm{s}} - 1}}{x\rho\sigma_{\mathrm{s}}} \tag{7}$$

For the coherent scattering neutron signal, the influence of the coherent scattering peaks can be reduced by increasing the neutron wavelength. The coherent scattering generated by the interaction between neutrons and the sample originates from the phase-coherent superposition of neutron waves. When the scattering process satisfies Bragg's law[36], diffraction peaks are formed:

$$2dsin\theta = n\lambda \tag{8}$$

Where d is the lattice spacing, λ is the neutron wavelength, and θ is the Bragg diffraction angle. In the non-Bragg scattering region where the neutron wavelength is sufficiently large that the above condition cannot be satisfied, coherent scattering contributes to the background in the form of a diffuse background and can be corrected using a matrix subtraction method.

Considering the Poisson statistical characteristics of neutron counting, the theoretical limit of detection of the system can be estimated based on the measured signal and measurement time. For a measurement time of t and a normalized scattering intensity of I, the statistical uncertainty of the neutron counts under the Poisson distribution satisfies $\sigma_I = \sqrt{I/t}$. Therefore, the theoretical limit of detection

(LOD)[36] can be expressed as follows:

$$\mathrm{LOD} = \frac{\sigma_{\Delta I}}{A} = \frac{\sqrt{{\sigma_{I_1}}^2 + {\sigma_{I_2}}^2}}{A} \tag{9}$$

For a conservative estimate, σ_{I_1} and σ_{I_2} are taken as the two largest statistical errors among the experimental results, respectively.

3. Apparatus Design

The experiments were carried out at the Small-Angle Neutron Scattering (SANS)[41] spectrometer on the C2 beamline of the China Mianyang Research Reactor (CMRR)[42], located at the Institute of Nuclear Physics and Chemistry, China Academy of Engineering Physics. The maximum power of the CMRR reaches 20 MW, generating a thermal neutron flux of 2.4×10^{14} n·cm^{-2}s^{-1} and a cold neutron flux of 10^9 n·cm^{-2}s^{-1}[43] for neutron scattering experiments.

Table 1. Performance parameters of the SANS instrument[41].

Performance Item	Technical Specifications
Wavelength Range	0.35-1.5nm
Wavelength Resolution	$\Delta\lambda/\lambda$:8%-12%
Scattering Vector Q Range	0.01-6.3 nm^{-1}
Flux at sample position （0.53 nm/20 MW）	1.18×10^7 cm^{-2}s^{-1}

The SANS instrument, shown in Fig. 3, with its main technical specifications listed in Table 1, is a powerful tool for non-destructive probing of nanoscale structures and is widely applied in basic science and engineering materials research. The selected neutrons enter a 10.5-meter-long collimation line to reach the three-dimensional sample stage, where they interact with the sample. The resulting scattered signals are captured by ^{3}He tube detectors, with the testing duration at each point being determined by the required neutron flux and contrast ratio.



Fig. 3. Small-angle neutron scattering.

The neutron nondestructive testing device developed in this study for sensitive hydrogen-content analysis exploits the exceptionally large neutron incoherent scattering cross section of hydrogen. A backscattering detector configuration was employed to avoid interference from intense forward-scattered background signals associated with the incident neutron beam. The ultrashort sample-to-detector distance of 150 mm substantially improved the measurement efficiency. In addition, a long-wavelength neutron mode with wavelengths greater than 6 Å was adopted to minimize the influence of differences in the intrinsic properties of the tested materials. This device addresses several key challenges encountered in conventional neutron

incoherent scattering-based hydrogen measurements, including intense scattered-neutron interference, background contributions, and poor measurement consistency arising from differences in material structure. Under the same neutron fluence and with detectors of the same size, the proposed configuration can significantly improve measurement efficiency. The device can be applied to nondestructive measurements of relative variations in hydrogen content in a wide range of materials. When combined with measurements using standard samples, it can also provide quantitative information on absolute hydrogen content. This approach therefore offers a new tool for applications including the investigation of hydrogen embrittlement in metals, the characterization of hydrogen-storage materials, and the evaluation of hydrogen-corrosion-resistant materials.

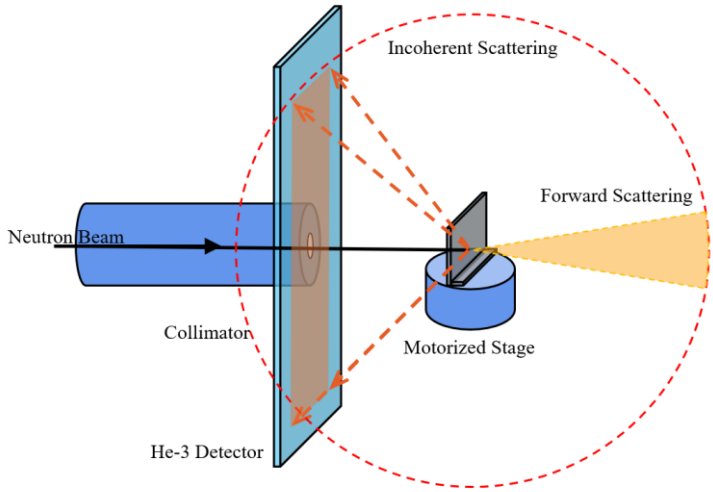


Fig. 4. Configuration of the incoherent scattering setup and detector arrangement. The sample is placed on the sample stage at a distance of approximately 150 mm from the ^{3}He detector. The detector consists of fifteen 2.54-inch ^{3}He tubes, providing an effective testing height of 600 mm.

4. Samples and Experimental Validation

Polypropylene (PP) thin films and zirconium alloys were selected as the subjects of this study. PP thin films possess high uniformity and a fixed H content[34], and the hydrogen content can be controlled by stacking multiple layers of films, making them an ideal carrier for technical validation experiments. For the zirconium alloy samples, the hydrogen content was controlled via hydrogen-charging experiments and quantitatively analyzed using Thermal Desorption Spectroscopy (TDS)[44] for verification. Both of these samples belong to materials with low absorption and low multiple scattering. After pretreatment, all samples were sealed in aluminum foil and fixed on the sample stage to be scanned one by one. Among them, for the PP film samples, Sample No. 0 contained no PP film, whereas Samples No. 1 to 4 were encapsulated with one to four pieces of PP films, respectively; for the Zircaloy samples (Samples 1 to 4), four Zircaloy pieces with different hydrogen contents were encapsulated.

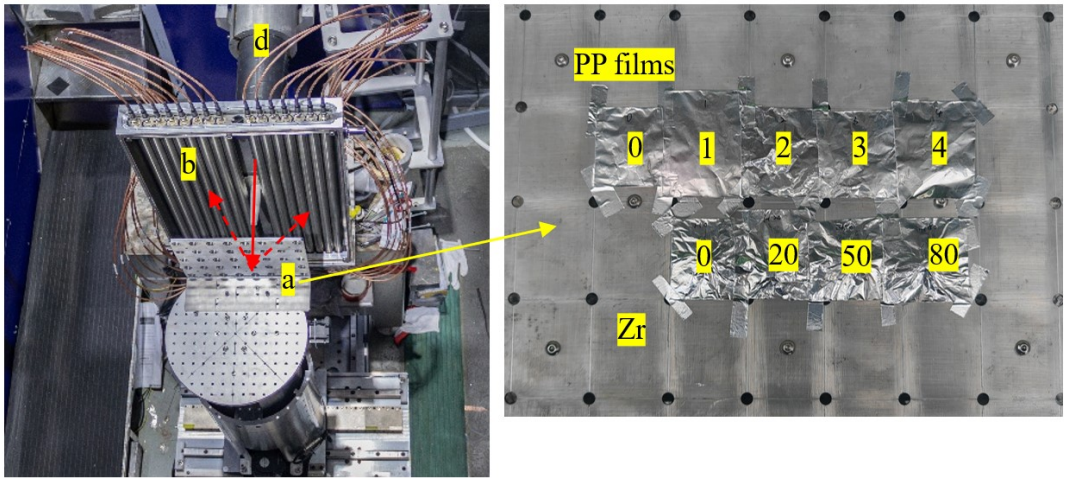


Fig. 5 Experimental configuration for neutron measurements, where the red arrows indicate the incident neutron beam direction and the scattering directions received by the detector: (a) Sample mounting arrangement on the stage plate, (b) ^{3}He detector, (c)Motorized Stage, (d) Collimator.

4.1. Experimental Setup for PP Thin-Film Samples

The chemical formula of the PP film is $(C_3H_6)_n$, corresponding to a hydrogen mass fraction w_H of approximately 14.29%. The samples had a diameter d_1 of 63.5 mm and a nominal thickness of 6 μm. To precisely account for the hydrogen content and evaluate sample consistency, four sample pieces were precisely weighed. As summarized in Table 2, the average mass of the PP samples m_{pp} was 0.016775 g/piece, with a maximum mass deviation of 3.7%. This deviation falls within an acceptable range for ultra-thin polymer films, demonstrating good sample uniformity. Consequently, it can be approximated that the thickness and density distributions are consistent. Under this assumption, the hydrogen content of the PP sample within the neutron beam irradiation area is given by:

$$m_{\mathrm{H}} = w_{\mathrm{H}} \cdot m_{\mathrm{pp}} \cdot \frac{{d_2}^2}{{d_1}^2}, \tag{10}$$

The maximum lattice spacing of the sample (110 plane) is approximately 6.2 Å[45, 46], so the neutron wavelength is selected as 7.2 Å to avoid the neutron diffraction signals on the detector, and the incident beam-limiting aperture diameter d_2 is adjusted to 2 mm. Under these conditions, the scattering signal is predominantly dominated by incoherent scattering positively correlated with hydrogen content, while coherent scattering manifests only as a weak structural background. Based on the above parameters, the mass of hydrogen participating in scattering within the neutron beam irradiation area for a single sample is approximately 2.355 μg.

Table 2. Mass measurements of PP thin film samples.

Sample No.	Mass (g)	Mass Deviation (%)
1	0.0168	1.08
2	0.0169	1.7
3	0.0167	0.5
4	0.0167	0.5

4.2. Experimental Setup for Zirconium Alloy Samples

The zirconium alloy samples were Zr-2.5Nb hydrogen reference materials prepared by the Institute of Machinery Manufacturing Technology, China Academy of Engineering Physics[47]. These reference materials were fabricated via the gas-phase absorption method using Zr-2.5Nb alloy strips as the substrate. The substrate was first dehydrogenated at 1100 °C under high vacuum for 120 min to remove residual hydrogen in the material; subsequently, quantitative H_2 gas was introduced within the temperature range of 650–850 °C for gas-phase absorption. Finally, homogenization was performed at 400 °C for 24 h to ensure a uniform distribution of hydrogen throughout the sample[44].

The hydrogenation system employed a gas-phase hydrogen charging apparatus. The system consisted of a high-vacuum system, a constant-volume gas charging system, a pressure measurement system, and an infrared heating device. The amount of hydrogen introduced was precisely controlled using the pressure–volume–temperature (PVT) method, while the hydrogen absorption process was monitored through changes in pressure. Thermal desorption spectroscopy coupled with quadrupole mass spectrometry (TDS-QMS) was used to verify the accuracy of hydrogen charging methods. Four Zr-2.5Nb alloy samples with a nominal hydrogen concentration of 20 ppm were prepared. After hydrogen charging, the measured everage hydrogen content of the sample was 20.20 ppm, with a relative standard deviation of 5.3%. Subsequently, samples with theoretical hydrogen contents of 50 ppm and 80 ppm were further prepared using the PVT method for the incoherent scattering experiments.

Table 3. Measurement results of hydrogen content in Zr alloy samples.

Sample No.	Sample Mass (g)	hydrogen content (ppm)	Mass Deviation (%)
1	0.2014	20.43	1.25
2	0.2340	19.07	5.49
3	0.1809	21.53	6.70
4	0.2009	19.68	2.47

5. Experimental Results and Analysis

5.1. Experimental Results

Table 4 summarizes the neutron incoherent scattering measurement results for

the PP film samples. In the absence of PP films sealed in the aluminum foil, the initial normalized neutron count rate was 63.17, which primarily originated from the ambient background and air scattering. As the number of PP films increased, the measured neutron count rate increased accordingly, agreeing well with the experimental expectations.

Table 4. Results of neutron incoherent scattering measurements.

Number of PP films	Hydrogen mass in the irradiated region (μg)	Normalized neutron count rate (a. u.)	Statistical error (a. u.)
0 (Al foil only)	0	63.17	0.33
1	2.355	73.32	0.35
2	4.710	83.42	0.37
3	7.065	94.83	0.39
4	9.412	105.10	0.42

Fig. 6 shows the curve of the neutron count rate for the PP film samples as a function of sample hydrogen content. As observed from the figure, the neutron count rate is linearly proportional to the hydrogen content in the samples. Fitting the experimental data with a linear function yields the scaling relationship between the neutron count rate and hydrogen content for the present experimental layout, with a fitted slope of 4.483 μg^{-1}. All experimental data points lie on the fitted curve, indicating that the neutron incoherent scattering method can provide reliable quantitative measurements over the hydrogen-content range investigated in this study.

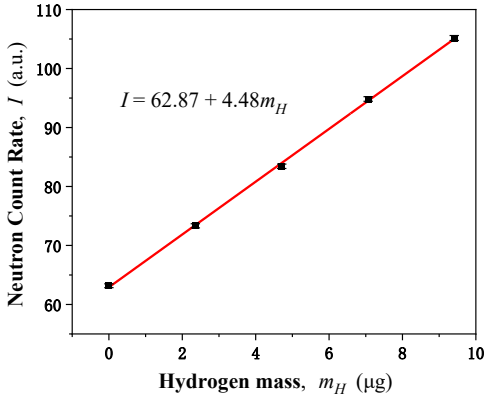


Fig. 6. Neutron count rate versus hydrogen mass curve.

To ensure that the neutron beam accurately covers small-sized samples, the crosshair scan method was employed for testing the zirconium alloy samples. By comparing the count distributions in both horizontal and vertical directions, the peak data where signal intensity reached a saturated plateau were selected as the effective neutron incoherent scattering counts for the samples. Each sample point was scanned for 180 s to ensure sufficient measurement accuracy. The neutron counting results for the zirconium alloy samples are summarized in Table 5:

Table 5. Results of neutron incoherent scattering measurements.

Zr Sample ID	Hydrogen content in the irradiated region (ppm)	Normalized neutron count rate (a. u.)	Statistical error (a. u.)
1	0.00	123.65	0.83
2	20.20	134.12	0.86
3	50.50	143.39	0.89
4	80.80	154.71	0.93

Fig. 7 shows the variation in neutron count rate as a function of the hydrogen content in the zirconium alloy samples. As can be seen from the figure, the neutron count rate exhibits a linear relationship with the hydrogen content in the samples. Linear fitting of the experimental data provides the calibration relationship between the neutron count rate and hydrogen content for the present experimental configuration. The fitted slope was 0.3779 ppm^{-1}, and the theoretical LOD reached 3.3 ppm. These results demonstrate that the neutron incoherent scattering method also provides good quantitative performance for determining the hydrogen content in zirconium alloys.

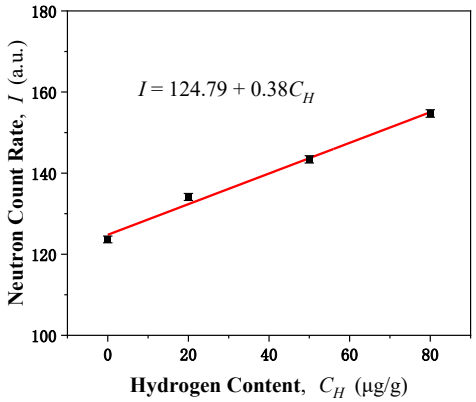


Fig. 7. Neutron count rate versus hydrogen content curve.

5.2. Analysis

The measurement results obtained from the PP thin-film samples first validate the stability and quantitative measurement capability of the proposed method. Polymer materials with well-defined chemical compositions have been widely used as standard or reference samples in neutron experiments because of their stable elemental composition and good homogeneity[48, 49]. In this study, the mass deviation among the PP thin-film samples was within 3.7%, indicating good consistency among the samples. On this basis, the good linear relationship observed between the normalized neutron count rate and hydrogen mass demonstrates that the measurement system responds reliably to the incoherent scattering signal from hydrogen, rather than to random variations caused by differences in sample composition. The sensitivity coefficient obtained in this experiment was 4.483 μg^{-1}. These results

further demonstrate that the designed measurement device can stably extract the incoherent scattering signal generated by hydrogen and convert it into a quantitative measurement signal.

Research on hydrogen-content analysis in materials using neutron scattering techniques has evolved from indirectly obtaining hydrogen-related information by suppressing or excluding incoherent scattering signals in conventional neutron scattering instruments to actively extracting hydrogen incoherent scattering as the primary signal of interest. Previous studies[36] have demonstrated that hydrogen content can be determined using neutron diffraction by separating and analyzing hydrogen-related incoherent scattering information contained in the scattering background, with a theoretical detection limit on the order of 10 ppm . However, conventional neutron diffractometers are primarily designed to obtain coherent diffraction information from materials. The incoherent scattering signal generated by hydrogen is therefore generally superimposed on a complex scattering background, making signal extraction and quantitative analysis dependent, to some extent, on background fitting and data-processing methods. Subsequently, studies by Yan et al.[37] based on small-angle and wide-angle incoherent neutron scattering further extended this approach. Wide-angle incoherent scattering can, to some extent, reduce or separate the influence of scattering arising from the intrinsic structure of the material, such as oxide layers, on the hydrogen incoherent scattering signal, thereby facilitating the identification of hydrogen-related signals and enabling detection limits on the order of 10 ppm. These studies have demonstrated the feasibility of quantitative hydrogen-content analysis using neutron incoherent scattering. Nevertheless, the neutron collection efficiency of existing scattering instruments can still be significantly affected by detector geometry and the sample-to-detector distance. In addition, the separation of incoherent scattering signals can be further optimized through the use of long-wavelength neutrons. Therefore, there remains considerable potential for improving measurement sensitivity and stability through dedicated optimization of the instrument configuration and neutron wavelength selection according to the characteristics of hydrogen incoherent scattering.

The experimental results of this study further demonstrate that structural optimization specifically targeting the incoherent scattering characteristics of hydrogen is an effective approach for improving measurement performance. First, the use of long-wavelength neutrons effectively reduces the influence of coherent diffraction signals from crystalline materials, thereby minimizing interference arising from differences in the intrinsic structure of the materials. Second, the backscattering detector configuration avoids the propagation direction of the incident neutron beam and thus reduces, to some extent, interference from intense scattering signals such as transmitted neutrons and forward small-angle scattering. This configuration provides a relatively independent angular range for detecting the hydrogen incoherent scattering signal. Finally, because the detector is less affected by intense forward-scattered signals, it can be positioned closer to the sample, reducing the sample-to-detector distance within 200 mm. This configuration increases the hydrogen signal intensity by nearly a factor of 50, substantially improving the

effective collection efficiency of hydrogen-related signals and thereby enhancing both measurement efficiency and hydrogen-content sensitivity. Collectively, these design strategies enable more efficient and sensitive detection of hydrogen through incoherent neutron scattering, providing an improved approach for subsequent quantitative hydrogen-content measurements.

Although the setup developed in this work enhances the measurement efficiency and quantitative sensitivity of incoherent neutron scattering signals from hydrogen, this approach is still subject to certain operational constraints and limitations in information retrieval. Because incoherent scattering does not retain the phase and structural information provided by coherent scattering, this method cannot readily distinguish between solid-solution hydrogen, hydride precipitates, and hydrogen residing in distinct local environments. Consequently, the present method is best suited for rapid, non-destructive quantification of total hydrogen content, rather than microstructural characterization such as site occupation analysis or hydride phase identification.

6. Conclusion

In this study, a neutron scattering apparatus for non-destructive testing of hydrogen was developed. By employing a backscattering detector configuration and the long wavelength neutron beam, the device minimizes the interference from material crystal diffraction signals and forward neutron small-angle scattering signals. The above setups allow for further reduction of the sample-to-detector distance (within 200 mm), thereby significantly improving test sensitivity and efficiency. Under the same neutron fluence and using detectors of the same size, the proposed configuration can improve the measurement efficiency by nearly a factor of 50. Thereby, the device addresses the major challenges encountered in conventional neutron incoherent scattering measurements of hydrogen content, including intense stray-neutron and background interference as well as poor measurement consistency caused by differences in material structure.

Measurements of polypropylene and zirconium alloy samples demonstrated an excellent linear relationship between the neutron count rate and hydrogen content, confirming the feasibility of the proposed method for quantitative hydrogen-content measurements in materials. The calculated results indicate that the device exhibits high sensitivity to hydrogen, with a theoretical limit of detection of 3.3 ppm, outperforming previously reported neutron-based hydrogen measurement techniques. The proposed incoherent scattering technique enables rapid measurements while preserving sample integrity, which provides a new measurement approach for the development and mechanistic investigation of hydrogen-corrosion-resistant materials.

Acknowledgment

Project NST20240203 supported by National Key Laboratory of Neutron Science and Technology.

National Natural Science Foundation of China No. 12427811.

References

1. Dupont J 2018 *Chem. Eur. J.* **25** 3404

2. Adamson S P, Orman S, Picton G 1969 *J Nucl Mater* **33** 215
3. Severens R J, Brussaard G J H, van de Sanden M C M, Schram D C 1995 *Appl Phys Lett* **67** 491
4. Lenzen M, Collins R E, Prince K 2005 *J. Non-Cryst. Solids* **351** 317
5. Weiss Z 2021 *Hydrogen* **2** 225
6. Ritchie A G, Greenwood R C, Randles S J, Netherton D R, Whitehorn J P 1986 *J Nucl Mater* **140** 197
7. Von Zeppelin F, Haluška M, Hirscher M 2003 *Thermochim Acta* **404** 251
8. Chiu Y C, Chen B Y, Hsu C C, Tsai C W, Wang S M, Chang I L, Chang C W 2025 *ACS Nano* **19** 10070
9. Martin T L, Coe C, Bagot P A, Morrall P, Smith G D, Scott T, Moody M P 2016 *Sci Rep* **6** 25618
10. Siekhaus W J, Weber P K, Hutcheon I D, Matzel J E P, McLean W 2015 *J Alloys Compd.* **645** S225
11. Ji H, Wu H, Pan Q, Cai D, Meng X, Chen X, Shi P, Wang X 2019 *npj Mater. Degrad.* **3** 9
12. Du J P, Geng W T, Arakawa K, Li J, Ogata S 2020 *J Phys Chem Lett* **11** 7015
13. Gault B, Saksena A, Sauvage X, et al. 2025 *Microsc. Microanal.* **30** 1205
14. Krüger S E, Rebello J M A, de Camargo P C 1999 *NDT & E Int.* **32** 275
15. Wang X, Fu X, Zhao Z 2003 *Surf Rev Lett* **10** 325
16. Wilde M, Ohno S, Ogura S, Fukutani K, Matsuzaki H 2016 *J. Vis. Exp.* **109** 1
17. Lin H-J, Li H-W, Shao H, Lu Y, Asano K 2020 *Mater. Today Energy* **17** 100463
18. Miao Y, Cross T A, Fu R 2014 *J Magn Reson* **245** 105
19. Weick S, Grosse M 2024 *Materials* **17** 781
20. Grosse M, van den Berg M, Goulet C, Lehmann E, Schillinger B 2011 *Nucl. Instrum. Methods Phys. Res. A* **651** 253
21. Callori S, Rehm C, Causer G, Kostylev M, Klose F 2016 *Metals* **6** 125
22. Kofu M, Hashimoto N, Akiba H, Kobayashi H, Kitagawa H, Tyagi M, Faraone A, Copley J R D, Lohstroh W, Yamamuro O 2016 *Phys. Rev. B* **94** 064303
23. Heuser B J, Prisk T R, Lin J L, Dax T J, Zhang Y 2019 *J Nucl Mater* **518** 177
24. Grosse M, Schillinger B, Kaestner A 2021 *Appl. Sci.* **11** 5775
25. Yan Y, Plummer L K, Ray H, Cook T, Bilheux H Z 2014 *Mater. Res. Soc. Symp. Proc.* **1645** 248
26. Grosse M, Roessger C, Stuckert J, Steinbrueck M, Kaestner A, Kardjilov N, Schillinger B 2015 *Phys. Procedia* **69** 436
27. Strobl M, Manke I, Kardjilov N, Hilger A, Dawson M, Banhart J 2009 *J Phys D: Appl Phys* **42** 243001
28. Agüi-Gonzalez P, Jähne S, Phan N T N 2019 *J Anal At Spectrom.* **34** 1355
29. Reif B, Ashbrook S E, Emsley L, Hong M 2021 *Nat Rev Methods Primers.* **1** 2
30. Stevie F A, Donley C L 2020 *J. Vac. Sci. Technol. A* **38** 063204
31. Gault B, Chiaramonti A, Cojocaru-Miredin O, Stender P, Dubosq R, Freysoldt C, Makineni S K, Li T, Moody M, Cairney J M 2021 *Nat Rev Methods Primers.* **1** 51
32. Yan Y, Qian S, Garrison B, Smith T, Kim P 2018 *J Nucl Mater* **502** 191
33. Shukla S, Singh P, Roy T, Kashyap Y S, Shukla M, Singh R N 2021 *J Nucl Mater*

544 152679
34. Choi Y N, Oh H S, Em V T, Somenkov V A, Lee C H, Park S D 2002 *Appl. Phys. A* **74** s1710
35. Singh S 2023 *Neutron Reflectometry: a technique for revealing emergent phenomena at interfaces in heterostructures* (London, England: IOP Publishing)
36. Fritzsche H, Huot J, Fruchart D 2016 *Neutron Scattering and Other Nuclear Techniques for Hydrogen in Materials* (Cham, Switzerland: Springer International Publishing)
37. Yan Y, Qian S, Littrell K, Parish C M, Plummer L K 2015 *J Nucl Mater* **460** 114
38. Shibayama M, Matsunaga T, Nagao M 2009 *J Appl Crystallogr* **42** 621
39. Kvardakov V V, Chen-Mayer H H, Mildner D F R, Somenkov V A 1998 *J Appl Phys* **83** 3876
40. Shibayama M, Nagao M, Okabe S, Karino T 2005 *J Phys Soc Jpn* **74** 2728
41. Tang Y F, Zhong S Y, Yan G Y, Chen J 2023 *JINST* **18** P09032
42. Tang Y, Zhong S, Yan G, Chen J 2023 *J Appl Crystallogr* **56** 1252
43. Wang G, Qian D, Ma J, Li R, Yuan S, Leng J, Dou H, Tang B 2019 *Ann Nucl Energy.* **130** 124
44. Li J, Zhang F, Tang D, Chen Y, Shen X, Liu D 2025 *Vacuum* **241** 114636
45. Karacan İ, Benli H 2011 *Tekstil ve Konfeksiyon* **21** 201
46. Alcazar D, Ruan J, Thierry A, Lotz B 2006 *Macromolecules* **39** 2832
47. Zhang T, Zhang F, Lin N, Zhu J, Peng X, Wang M, Jin W, Li Q, Wu J, Liu X, Chen C, Liu D, Zhao W, Ye X, Gui C 2026 *Vacuum* **250** 115335
48. Soles C L, Douglas J F, Wu W-l, Dimeo R M 2003 *Macromolecules* **36** 373
49. Higgins J S 2016 *Annu Rev Chem Biomol Eng.* **7** 1